Engineering Applications of Artificial Intelligence 120 (2023) 105834

Contents lists available at ScienceDirect

Engineering Applications of Artificial Intelligence

journal homepage: www.elsevier.com/locate/engappai

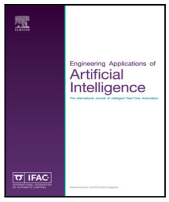

Data-driven failure prediction of Fiber-Reinforced Polymer composite materials

Allyson Fontes *, Farjad Shadmehri

Concordia Center for Composites (CONCOM), Department of Mechanical, Industrial and Aerospace Engineering, Concordia University, Montreal, QC, Canada
Research Center for High Performance Polymer and Composite Systems (CREPEC), Montreal, Quebec, Canada

ARTICLE INFO

Keywords:
Deep Neural Networks (DNN)
Failure strength prediction
Data-driven modeling
Polymer composite materials

ABSTRACT

The present study illustrates the effectiveness of Deep Neural Networks (DNN) as a tool for creating a data-driven failure model for Fiber-reinforced Polymer (FRP) composite materials. Experimental failure data presented in the literature for laminates tested under biaxial and triaxial stresses were used to develop the data-driven model. A fully connected DNN with 20 input units and 1 output unit trained with a constant learning rate. The network's inputs describe the laminate layup sequence, lamina properties, and the loading conditions applied to the test specimen, whereas the output is the length of the failure vector. The failure boundaries generated by the DNN were compared to conventional theories such as the Tsai–Wu, Cuntze, and Pinho theory. The data-driven model's predictions are found to fit the experimental data better than the conventional theories. The DNN's ability to fit higher-order polynomials to data makes it an effective tool for predicting the final failure of FRP composite laminates.

1. Introduction

Fiber-reinforced polymer (FRP) composite materials' high stiffness, high strength, and lightweight characteristics make them the preferred choice for advanced applications. However, despite their widespread use, there is a fundamental gap in knowledge surrounding their failure prediction. Conventional analytical failure theories developed to date (e.g., Tsai and Wu, 1971) are unable to predict failure with high precision. An investigation into the accuracy of composite failure theories, known as the World-Wide Failure Exercise (WWFE), concluded that none of the theoretical models could predict the final failure within ±10% of the experimentally measured strengths in 40% of the test cases (Soden et al., 2004). The discrepancies between theories' predictions and experimental data are due to the complex nature of the failure phenomenon in composites and the fact that many factors (e.g., manufacturing methods, and process parameters) can affect the failure.

This inability to predict failure analytically necessitates extensive experimental tests, which require large monetary and time investments, to determine the strength and sizing of FRP composite components. In recent years, Machine Learning (ML) techniques have gained popularity within many engineering disciplines. Specifically, within the field of composite materials, the ML algorithm known as Deep Neural Network (DNN) shows potential for simulating and solving complex problems (Sapuan and Mujtaba, 2009). Notably, the algorithm is emerging as a time-efficient technique for assisting with composite design (e.g., predicting material properties), process optimization (e.g., predicting relationships between manufacturing conditions and final part quality), and property analysis (e.g., predicting dynamic mechanical properties) Sapuan and Mujtaba, 2009.

Due to their ability to learn relationships from data, neural networks have been applied for cure cycle optimization (Aleksendrić et al., 2016; Humfeld et al., 2021; Niaki et al., 2021), defect detection (Stamopoulos et al., 2018; Tang et al., 2022), in-situ Automated Fiber Placement process modeling (Islam et al., 2022; Wanigasekara et al., 2021, 2020), and fatigue life prediction (Al-Assadi et al., 2010; Fernández et al., 2022), to name a few. More precisely, studies have been conducted to determine the applicability of neural networks for predicting the failure strength of FRP composites. First, Labossière and Turkkan (1993) applied neural networks to predict the failure of fiber-reinforced paperboard composite laminae under plane stress conditions. They found that the DNN adapted well to the variations in the experimental data and advised that many experimental data points are required to achieve acceptable accuracy. In another study, Lee et al. (1999) used a DNN to predict the failure strength of cross-ply T300 carbon/epoxy laminates under biaxial loading. Their DNN was found to have higher predictive accuracy than the Tsai–Wu criterion; however, predictions can only be made for one material system. Seyhan et al. (2005) conducted compressive tests on E-glass/polyester fabrics made using Vacuum-Assisted Resin

* Corresponding author at: Concordia Center for Composites (CONCOM), Department of Mechanical, Industrial & Aerospace Engineering, Concordia University, Montreal, QC, Canada.
E-mail addresses: allyson.fontes@concordia.ca (A. Fontes), farjad.shadmehri@concordia.ca (F. Shadmehri).

https://doi.org/10.1016/j.engappai.2023.105834
Received 27 September 2022; Received in revised form 29 November 2022; Accepted 5 January 2023
Available online 28 January 2023

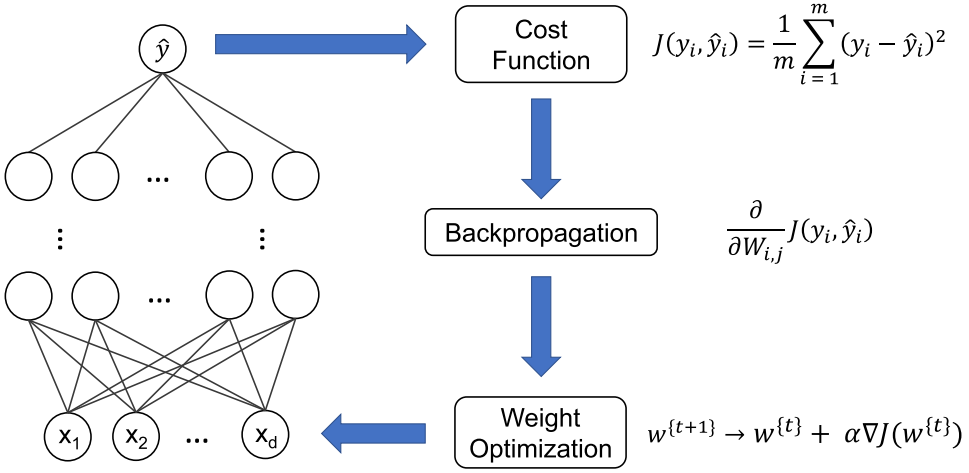

Fig. 1. Schematic of the neural network training process.

Transfer Molding (VARTM) to better understand the effect mechanical properties have on VARTM composites. They then trained a neural network to predict the compressive strength and concluded the predictions were consistent with experimental observations. It was noted that the number of training data points has a significant effect on the predictive quality. Chen et al. (2021) coupled a micromechanics-based representative volume element finite element model with a neural network to predict the failure of triaxially loaded IM7/8552 lamina. The developed neural network model achieved more than 97.5% accuracy on the finite element generated data. The authors conclude by proposing the development of a neural network-based failure criterion to replace conventional analytical criteria.

Bayesian Neural Networks (BNN) are an alternative modeling approach that provide an uncertainty estimate with their predictions. Training algorithms such as Bayes by Backprop, Hamiltonian Monte Carlo, and Approximate Bayesian Computation are a few examples of inference approaches that have been used to train a BNN for uncertainty estimation in fatigue prediction of composites (Fernández et al., 2022). For strength prediction, Fan and Wang (2014) used a probabilistic neural network (PNN) to predict the tensile strength of open-hole T800/epoxy specimens. The PNN predicted the occurrence of failure within ±4% error on a limited number of experimental results. The authors stated that the model could be extended to make predictions on other composite structures with variability in the experimental data.

Thus, as established by the above-mentioned studies, DNNs can learn the complex non-linear relationships that exist between the laminate and loading conditions and effectively predict the final failure of composite materials. However, the above-mentioned studies have focused on predicting the strength of one specific material system, laminate, or loading scenario. Therefore, the resulting network is only applicable to one setup and cannot generalize to include additional experimental data. Most recently, Fontes and Shadmehri (2021) addressed this shortcoming by developing a DNN that can predict the failure strength for a variety of laminates and material systems. Although their model successfully predicts final failure for multiple laminates, the approach cannot be extended to include any layup sequence or triaxial loading conditions. Their inputs limit the prediction to a finite number of laminate angles, and the stacking sequence is not considered.

The present study addresses the limitations of the previous studies by developing a DNN-based framework with generalized input features that provide the flexibility to accept any ply angle while encoding information about ply sequencing. Furthermore, the proposed framework expands the data set and input features to predict failure for triaxial loading scenarios. In other words, this study evaluates neural networks as an alternative to conventional analytical failure criteria by gathering data available in the literature. The goal is to assess whether a neural network can predict the failure strength for different laminates and various test cases. The method implemented to train the data-driven model using experimental data available in the literature is described. Furthermore, the network's predictive performance is compared and evaluated against predictions made by traditional failure criteria.

2. Methodology

The following section outlines the methods employed to develop the data-driven model. The experimental data selected for the model is described along with the steps taken to prepare the data, and the methodology used to train and evaluate the data-driven model.

2.1. Experimental data

Experimental data presented in three publications were used to develop the data-driven model. The data from the first World-Wide Failure Exercise (WWFE-I) (Hinton et al., 2004) and Lee et al. (1999) publications were curated to make up the biaxial loading portion of the data. In addition, the experimental results from the second World-Wide Failure Exercise (WWFE-II) (Hinton and Kaddour, 2012) were selected since they encompass triaxial loading conditions. Together, this collection of experimental data covers a range of commonly used laminates and loading scenarios. The following section outlines the details related to the laminates and the test cases selected from the above-mentioned publications.

The experimental data selected from the WWFE-I encompasses 5 laminates with continuous fibers tested under biaxial conditions (Soden et al., 2004a,b). A total of 287 experimental data points were taken from tests conducted on tubular specimens. All specimens in this study were tested until failure at a constant stress ratio (SR). Table 1 summarizes the laminates included in the study and their corresponding loading condition (Soden et al., 2004a). Next, the experimental data generated by Lee et al. (1999) includes 43 data points of cross-ply T300 carbon/epoxy tubular laminates tested under biaxial loading of axial and shear stress. Up to 5 specimens were tested at fixed biaxial SRs of axial to shear stress (σ_x:τ_{xy}). The eleven SRs evaluated are 0:1, 1:1, 2:1, 5:1, 10:1, 20:1, ±∞, −2:1, −5:1, and −10:1. Full details about the composite material and the experimental procedure are described in Lee et al. (1999).

The lamina strength properties for the WWFE-I material systems may be found in Soden et al. (2004a). For the development of the model, the materials are assumed to be transversely isotropic. As such, the out-of-plane material properties are assumed to be equal to the transverse material properties since they are not explicitly provided (i.e., $\sigma_2 = \sigma_3$ and $\tau_{12} = \tau_{13} = \tau_{23}$). As with the WWFE-I materials, the

Table 1
The laminates, materials, and loading test cases.

Dataset	Test case	Laminate	Material	Loading	No. points
WWFE-I (Soden et al., 2004a)	1	0°	E-glass/ LY556 epoxy	σ_y versus τ_{xy}	16
	2	0°	T300/BSL914C epoxy	σ_x versus τ_{xy}	34
	3	85°	E-glass/MY750 epoxy	σ_x versus σ_y	21
	4	(90°/±30°/90°)	E-glass/LY556 epoxy	σ_x versus σ_y	47
	5	(90°/±30°/90°)	E-glass/ LY556 epoxy	σ_x versus τ_{xy}	44
	6	(0°/±45°/90°)	AS4/3501-6	σ_x versus σ_y	43
	7	(±55°)	E-glass/MY750 epoxy	σ_x versus σ_y	82
Lee et al. (1999)	8	(0°/90°)	T300/epoxy	σ_x versus τ_{xy}	43
WWFE-II (Kaddour and Hinton, 2012)	9	0°	T300/PR319	$\sigma_1 = \sigma_2 = \sigma_3$ versus τ_{12}	21[a]
	10	90°	T300/PR319	$\sigma_1 = \sigma_2 = \sigma_3$ versus τ_{12}	21[b]
	11	90°	E-glass/MY750 epoxy	σ_2 versus σ_3 ($\sigma_1 = \sigma_3$)	18[c]
	12	0°	S-glass/epoxy	σ_1 versus σ_3 ($\sigma_2 = \sigma_3$)	22[d]
	13	0°	A-S carbon/epoxy	σ_1 versus σ_3 ($\sigma_2 = \sigma_3$)	14
	14	(±35°)	E-glass/MY750 epoxy	σ_y versus σ_z ($\sigma_x = \sigma_z$)	11
	15	(0°/90°/±45°)	IM7/8551-7	σ_z versus τ_{yz} ($\sigma_x = \sigma_y = 0$)	14
	16	(0°/90°)	IM7/8551-7	σ_z versus τ_{yz} ($\sigma_x = \sigma_y = 0$)	8

No. points after data pre-processing (Section 2.3.2):
[a]9.
[b]7.
[c]9.
[d]13.

T300 carbon/epoxy material used by Lee et al. is assumed to be transversely isotropic. Lee et al. did not report the transverse compressive strength (σ_{2C}) of the material. Therefore, the transverse compressive strength from the WWFE-I T300 carbon/epoxy was assigned to this material.

The experimental data presented in the WWFE-II contains data for continuous FRP composites subjected to 3D states of stress (Kaddour and Hinton, 2012; Hinton and Kaddour, 2013). Five types of orthotropic laminates with different combinations of fibers and matrices were used for this exercise. Table 1 includes the laminates and loading conditions from the original publication (Kaddour and Hinton, 2012). For uniformity across all experimental data, the WWFE-II test cases given in the principal material coordinate system (i.e., 1-2-3 coordinates) are translated into the global coordinate system (i.e., x-y-z coordinates). The test procedure used for the test cases with hydrostatic pressure is as follows: first, the pressure is applied to a predetermined value and then, the secondary load is monotonically increased until failure occurs.

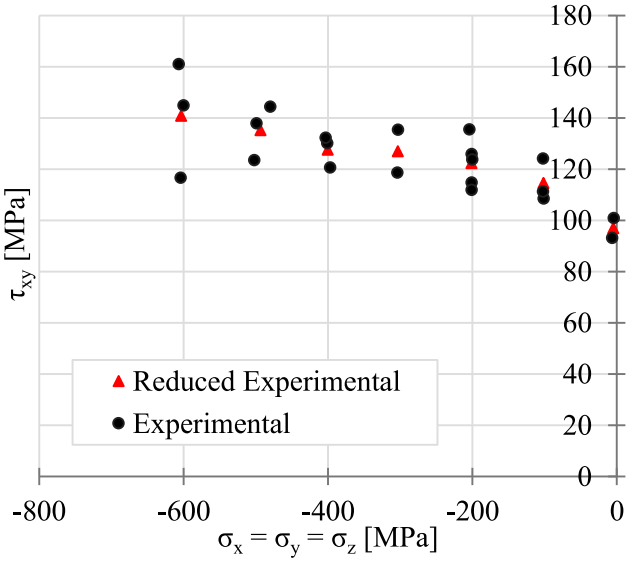

Fig. 2. WWFE-II test case 10 reduced experimental data used for model development.

2.2. Neural network overview

Neural networks are a supervised form of machine learning that discern complex non-linear relationships embedded in data (Gurney, 1997; Ketkar, 2017). Simple units with one input and one output are connected in series and in parallel to form the network structure. The connections between units in a network are learnable parameters called weights. These weights control the strength of the connection between the units, and ultimately, the network's output (Goodfellow et al., 2016). The optimal weights are found through a training process. During training, data (x_i) is passed to the network, and the network's prediction ($\hat{y}$) gets compared to the data's ground truth (y) via a cost function. Based on the error in the network's prediction, the backpropagation algorithm estimates the weight adjustments required to improve the predictions. An optimizer then updates all the weights, and the cycle (i.e., gradient descent) is repeated until the cost function reaches the convergence criterion. The iterative training cycle is schematically represented in Fig. 1.

The learning rate (α) is the hyperparameter that governs the step size the optimization algorithm takes when updating the weights. During training, the model must be monitored and prevented from overfitting the training data. This improves the model's ability to generalize to data points it has not previously seen. To achieve this, a technique known as regularization is implemented during training. The weight decay (λ) value is the regularization hyperparameter that governs how much the weights are penalized (Goodfellow et al., 2016). Both hyperparameters (i.e., α and λ) are tuned to the application.

2.3. Neural network implementation

2.3.1. Inputs and outputs

A DNN with an input layer of 20 units (i.e., d = 20 in Fig. 1) and 1 output unit was modeled. The input features to the network describe the laminate and the loading conditions applied to specimens. Specifically, the inputs define the laminae strength properties, the stress ratios, the order and orientation of the layup, and cases of symmetry. To be understandable by the DNN, the categorical symmetry input is mapped to an integer value. Table 2 outlines the 20 input features and illustrates an example of the raw input data for a $(0°/\pm45°/90°)_s$ specimen tested at a stress ratio of 0.75:1 (σ_x: σ_y). Additional examples of how the data was arranged before being fed into the neural network are provided in Appendix B.

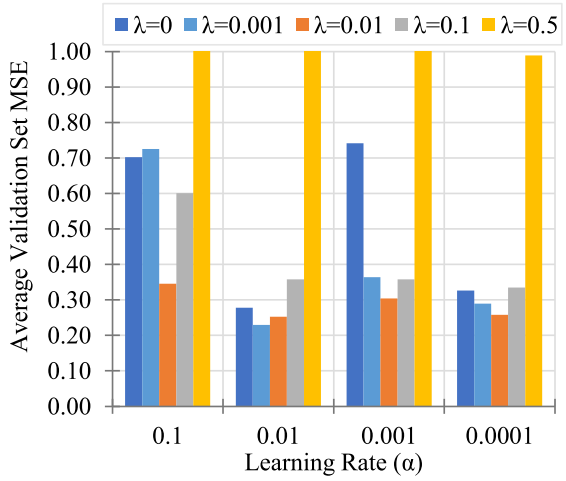

Fig. 3. Hyperparameter grid search results for the network with 3 hidden layers and 20 units per layer.

The stress ratio inputs play a critical role in the prediction of the failure strength. These 6 inputs are used to identify the relationship between the loaded axes, and they define whether loading is tensile or compressive. So, to improve the model's ability to learn relationships and generalize, a standard format is adopted. The stress ratio conventions implemented for the data-driven model are shown in Table 2. Take, for example, a specimen loaded axially (σ_x) and circumferentially (σ_y). If the specimen is loaded axially at a rate twice that of the circumferential load, a ratio of 2:1 (σ_x:σ_y) is passed to the network. Similarly, if the specimen is uniaxially loaded in axial compression or circumferential tension the inputs are −1:0 and 0:1, respectively. Note, all other stress ratio inputs are set to zero by default.

The format used to describe the laminate layup sequence is another key input. By inputting the layup in sequential order, the DNN can differentiate between laminates with the same ply angles in different stacking sequences. For example, the model can differentiate between the (0°/±45°/90°) and (0°/90°/±45°) laminates from the WWFE-I and the WWFE-II, respectively. Moreover, with this input format, any layup sequence can be passed to the network, and the inputs are not limited to the laminates available at the time of this study.

The length (L) of the failure vector is the only output of the network. The output is defined by the following equation:

$$L = \sqrt{\sigma_x^2 + \sigma_y^2 + \sigma_z^2 + \tau_{xy}^2 + \tau_{xz}^2 + \tau_{yz}^2} \tag{1}$$

where σ_x is the axial or longitudinal failure strength, σ_y is the circumferential or transverse failure strength, σ_z is the through-thickness failure strength, τ_{xy} is the in-plane shear failure strength, whereas τ_{xz} and τ_{zy} are the out-of-plane shear failure strengths.

Table 2
The neural network input features.

Category	#	Metric	Example
Lamina strengths [MPa]	1	σ_{1T}	1950
	2	σ_{1C}	1480
	3	σ_{2T}	48
	4	σ_{2C}	200
	5	σ_{3T}	48
	6	σ_{3C}	200
	7	τ_{12}	79
	8	τ_{13}	79
	9	τ_{23}	79
Cases of symmetry (S.)	10	No S. (0) Yes S. (1)	1
Stress ratios (σ_x:σ_y, σ_x:σ_z, σ_x:τ_{xy}, σ_y:τ_{xy}, σ_z:τ_{xy}, σ_z:τ_{yz})	11	σ_x	0.75
	12	σ_y	1
	13	σ_z	0
	14	τ_{xy}	0
	15	τ_{xz}	0
	16	τ_{yz}	0
Layup and orientation [degrees]	17	Ply 1	0
	18	Ply 2	+45
	19	Ply 3	−45
	20	Ply 4	90

2.3.2. Data preprocessing

Special care was taken when preprocessing the experimental data for test cases 9 to 12 listed in Table 1. As exemplified in Fig. 2, there are large variations in the experimental results for the tests conducted at pre-set pressures. Training on these raw experimental points would skew the neural network's ability to predict since the shear stress for a given pressure varies substantially (e.g., up to 40 MPa in Fig. 2). To mitigate this, these data were averaged, and the mean shear stress value was kept for the model development.

The experimental data were randomly divided into two subsets for k-fold cross-validation: the training–validation set (80%) and the test set (20%). Care was taken to ensure the 80–20 split was respected across all test cases. Then, the regression inputs (i.e., all inputs except the symmetry input) and the output data were standardized before training since they varied in magnitude. To achieve this, standardization was implemented for each data point ($x^{(i)}$) using the following equation:

$$x_d^{(i)} = \frac{(x_d^{(i)} - \mu_d)}{\sigma_d} \tag{2}$$

where μ is the mean and σ is the standard deviation of an input feature or output (d) calculated on the training–validation set.

2.3.3. Neural network architecture & training

A fully connected DNN was implemented on the "Google Colaboratoy", 2019 platform using "Python", 2018 and PyTorch, an open-source deep learning framework Paszke et al., 2019. The Adam optimization

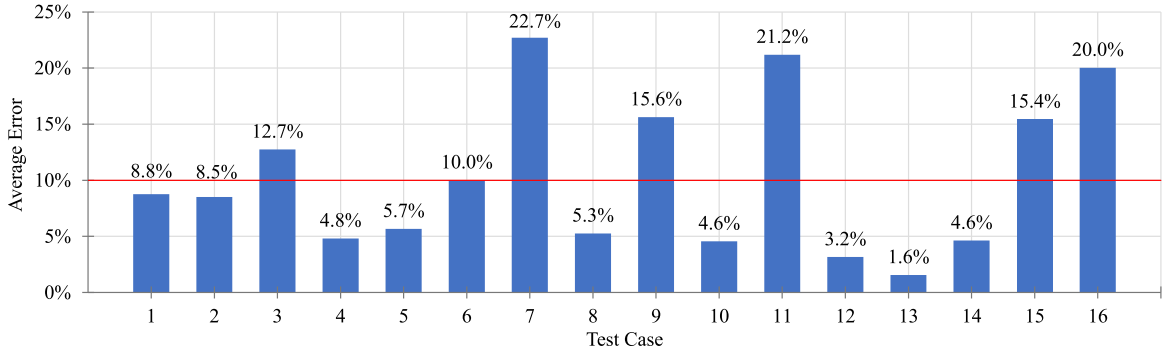

Fig. 4. The average error per test case. As outlined in Table 1, test cases 1–7 are from the WWFE-I, test case 8 is from Lee et al. and test cases 9–16 are from the WWFE-II.

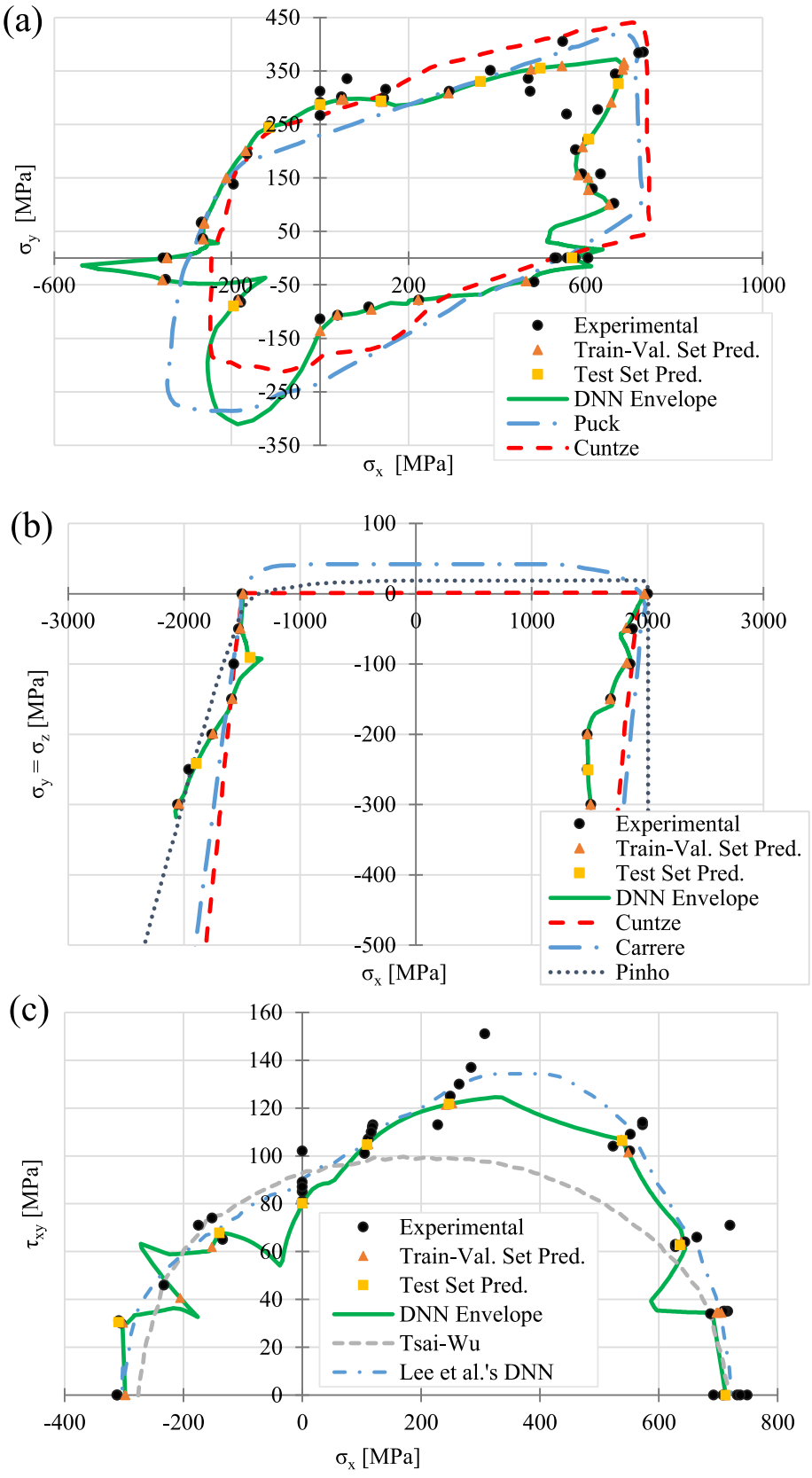

Fig. 5. Neural network experimental data and failure envelope predictions (pred.) compared to conventional failure criteria: (a) WWFE-I test case 4; (b) WWFE-II test case 13; (c) Lee et al. test case 8.

Table 3
The neural network parameters, architecture, and hyperparameters used for model implementation in PyTorch.

Metric	Value
Optimization algorithm	Adam
Activation function	ReLU
Cost function	MSE
Hidden layers	3
Units per hidden layer	20
Initial learning rate (α)	0.01
Weight decay (λ)	0.001
Epochs	8000

algorithm and the Rectified Linear Unit (ReLU) activation function were selected since they decrease training times. Adam optimizes the weights during training by using the exponentially weighted averages and the average squares of the past gradients, whereas the ReLU activation function takes the maximum value between 0 and the node's input (Goodfellow et al., 2016; Ketkar, 2017).

The mean squared error (MSE) was the cost function selected to compute the error of the network's predictions. L2 regularization, which reduces the network's overfitting by penalizing the weights and increasing the error value, was selected. The MSE cost function with L2 regularization included is defined as (Goodfellow et al., 2016):

$$J\left(y_i, \hat{y}_i\right) = \frac{1}{m}\sum_{i=1}^{m}\left(y_i - \hat{y}_i\right)^2 + \frac{\lambda}{2m}\sum_{l=1}^{L}\left\|w^l\right\|_2^2 \tag{3}$$

where m is the number of training data points, y_i is the data's ground truth, $\hat{y}_i$ is the network's prediction, λ is the weight decay, l is the layer number, L is the total number of layers, and $\|w^l\|_2^2$ is the L2 norm of the matrix of weights for a given layer (i.e., the square root of the sum of all squares of elements in the matrix).

As mentioned in Section 2.2, a model's hyperparameters must be manually adjusted for the application. Hyperparameter selection can be achieved using a variety of techniques. The two most common hyperparameter optimization algorithms are grid search and random search (Goodfellow et al., 2016; Raschka et al., 2022). Grid search is a brute-force search that examines each combination of hyperparameter values defined by the user. For this study, grid search optimization is selected since a small number of hyperparameters are tuned. A user-defined parameter grid was specified to select the learning rate, the weight decay value, the number of hidden layers, and the number of units per hidden layer. Network configurations with 2 to 3 hidden layers and 5, 10, and 20 units per hidden layer were evaluated. Simultaneously, learning rates ranging from 10^{-1} to 10^{-4} and weight decay values of 0, 0.5, 0.1, 0.01, and 0.001 were tested. Due to the limited number of available data, the grid search hyperparameter selection was coupled with the k-fold cross-validation method. Precisely, a 3-fold cross-validation resampling method was implemented to compare the performance of networks trained with different architectures and hyperparameter values. For each fold, a third of the train–validation set was randomly sampled to create a validation set and the remaining data were used to train a model. The combination of hyperparameter values that produced the average lowest MSE and the least variance on the validation sets was selected. Fig. 3 illustrates the results from the hyperparameter grid search for the network with 3 hidden layers and 20 units per hidden layer. Table 3 summarizes the hyperparameter values that resulted in the lowest MSE during k-fold cross-validation. These hyperparameters were used to train a model on the entire train–validation set for 8000 epochs with full batch gradient descent and weight decay using the Adam optimization algorithm.

3. Results and discussion

The following section presents the predictions made by the trained data-driven model. This section evaluates the model's average predictive accuracy and compares its predictions to existing analytical failure theories.

3.1. Neural network predictions

As above-mentioned, the DNN with 3 hidden layers and 20 units per hidden layer performed the best. With this architecture, the MSE reached a minimum value of 0.0358 on the train–validation data and 0.0362 on the test data. The predictions show good agreement with the experimental results. Further, the network did not overfit to locations where multiple specimens were tested with the same stress ratio. The error between each experimental point's true length and the model's prediction was calculated. The average error per test case is shown in Fig. 4.

As outlined in Fig. 4, the trained data-driven model predicted failure within 10% error on the Lee et al. dataset, in 70% of the test cases from the WWFE-I, and 50% of the test cases from the WWFE-II. Furthermore, the data-driven model predicted failure within 10% to 25% error in 30% of the test cases from WWFE-I and the remaining 50% of the WWFE-II test cases. This error rate is less than the errors reported for the failure theories presented in both WWFEs. In particular, the best conventional models presented in the WWFE-I were unable to predict the final strength of the multidirectional laminates within ±10% of the experimentally measured strengths in 40% of the test cases (Soden et al., 2004). For the WWFE-II, the best theories (Pinho, Carrere, Cuntze for Part B) predicted within ±10% of the experimentally measured strengths in 40% of the test cases, within ±10% and ±50% in 45% of the test cases, and below 50% or above 150% of the experimental strengths in the remaining 15% of the test cases (Kaddour and Hinton, 2013). Evidently, the DNN outperforms the conventional failure models on the experimental data.

Overall, the DNN's errors on the experimental data are within acceptable limits for this application. Most errors for the test cases are within 10%, which is a notable improvement compared to conventional failure theories. The elevated error for test case 7 of the WWFE-I data set is due to the scatter in the experimental data. For tests conducted at similar stress ratios, there are large variations in the failure lengths. The DNN predicts the mean length for these points, which increases the error on a point-by-point basis. Conversely, the larger errors for test cases 3, 9, 11, 15, and 16 are due to the limited amount of experimental data (see Table 1). The small number of experimental data points resulted in large gaps in the training data, which in turn, made it difficult for the network to learn the data's trend. Increasing the number of experimental data points for these test cases would improve the model's predictive ability. Combining a variety of test cases into one DNN may have limited the model's ability to generalize for these test cases with fewer data points. Thus, while the DNN developed in this work improves upon the predictions made by conventional failure theories, additional data would help decrease the errors across all the test cases.

3.2. Comparison with failure theories

Failure envelopes for all the laminates were generated using the trained DNN. The data-driven model successfully generalizes and predicts failure for data unseen during training. In other words, the boundaries generated by the DNN follow the general trends observed in the experimental data. The DNN's performance is benchmarked by comparing its failure envelopes to conventional theories.

The DNN's failure envelopes fit the WWFE-I experimental data more closely than the Kuraishi et al. (2004), Cuntze (2004), and Puck and Schürmann (2004) theories as reported in the WWFE-I. For instance, the DNN's average error for test case 2 was 8.5% which is approximately half of the average error of 16.6%, 14.9%, and 15.9% for Tsai–Wu, Cuntze, and Puck, respectively. Fig. 5a illustrates the DNN's failure envelopes for WWFE-I test case 4 compared to the envelopes generated by the conventional theories. The figure exemplifies the DNN's ability to learn the trend in the experimental data; however, it also shows the DNN's weakness for making predictions in regions

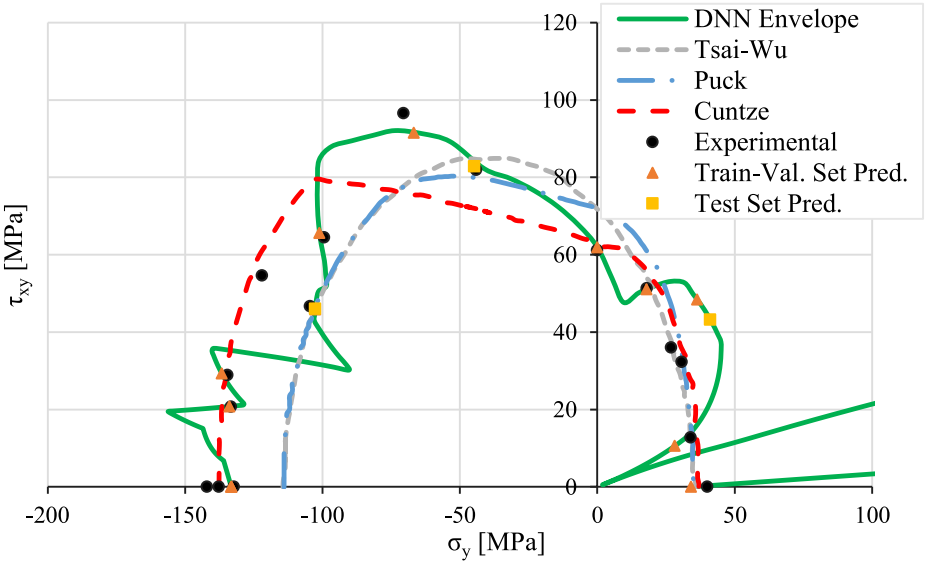

Fig. A.1. Neural network experimental data and failure envelope predictions compared to conventional failure criteria for WWFE-I test case 1.

where little experimental data is provided (i.e., quadrant 3). This emphasizes the need for experimental training data that covers the entire input space. Although generating enough experimental data requires an initial capital investment, the network's ability to generalize would reduce the experimental testing required in the long run.

As seen in Fig. 5a, the network's predictions in the transition region from uniaxial loading to biaxial loading around the stress ratio of infinity are inaccurate. The erroneous predictions in the transition region are due to the encoding of the stress ratios. The binary format used to differentiate the stress ratio of infinity (e.g., $\sigma_x/\sigma_y = \infty \rightarrow$ 1:**0**) and the biaxial stress ratio (e.g., $\sigma_x/\sigma_y = 10 \rightarrow$ 10:**1**) creates a discontinuity in the predicting function. The network is unable to learn a relationship between the uniaxial points and the location of the first biaxial experimental point. Notably, this issue does not arise for the transition from uniaxial loading with a stress ratio of 0 since the input in this region is continuous. For instance, the input for a stress ratio of 0 is **0**:1 and the first biaxial stress ratio could be **0.5**:1. Based on this behavior, the lack of experimental data within the transition region diminishes the network's prediction ability. It is recommended to limit the network's predictions to uniaxial cases and the region after the first biaxial experimental data point.

The DNN's failure envelopes for the WWFE-II data follow the trend in the experimental data more closely than the Cuntze (2013, 2012), Carrere et al. (2013, 2012) and Pinho et al. (2013, 2012) theories. As illustrated in Fig. 5b, the DNN successfully adapts to the non-linearity in the experimental data, whereas the conventional theories do not. This trend is observed for the WWFE-II test cases 12, 13, and 14 since they contain experimental data with stress ratios at evenly distributed intervals. As above-mentioned, for test cases 9, 11, 15, and 16, the limited number of experimental data points restricts the network's ability to interpolate and generate failure boundaries. The accuracy of predictions in-between the experimental data points for these test cases is diminished due to the gaps in the stress ratios.

Comparing the current work's boundary predictions to the envelope generated by Lee et al.'s network shows striking differences. The predictions for the experimental data points are similar (both ~5% error); however, the envelope generated by the current neural net is jagged between the experimental point locations (see Fig. 5c). It is hypothesized that Lee et al.'s paper has better predictions since it was trained to predict failure for a single laminate and so, the network's weights could be fine-tuned for that application. Unfortunately, the same fine-tuning could not be achieved for the current study due to the large data set. Due to the black-box nature of neural networks, it is difficult to identify the reason for the kinks in this failure boundary. Nevertheless, unlike this study's model, Lee et al.'s network cannot generalize and predict failure for laminates with any layup sequence.

4. Conclusion

In sum, the present study developed a DNN framework capable of improving upon the predictions of conventional analytical failure theories for several FRP composite laminates. The network can accept input data for a variety of layup sequences, material systems, and loading conditions. The results showed that a data-driven model can effectively predict the failure strengths of multiple types of laminates. The neural network's ability to fit higher-order polynomials to data allows it to fit the experimental data more effectively than conventional failure theories. However, the need for experimental data which covers the entire input space remains a key challenge. The number of experimental data points available for this study was a limiting factor of the neural network's prediction ability. Nonetheless, it is important to mention that the framework proposed in this study is designed to generalize for other test cases. That is, the inputs are formatted so that as additional experimental data becomes available, a neural network can be easily trained to predict failure for these new laminates and loading scenarios. Developing a data-driven failure theory with this framework can provide more precise estimates of the failure strength of FRP composite laminates. Once a model is trained on the desired material system(s) or laminate(s), it can be used for design to inform the strength and sizing of composite components.

CRediT authorship contribution statement

Allyson Fontes: Conceptualization, Methodology, Software, Validation, Formal analysis, Investigation, Writing – original draft, Writing – review & editing, Visualization. **Farjad Shadmehri:** Conceptualization, Methodology, Resources, Writing – review & editing, Supervision, Funding acquisition.

Declaration of competing interest

The authors declare that they have no known competing financial interests or personal relationships that could have appeared to influence the work reported in this paper.

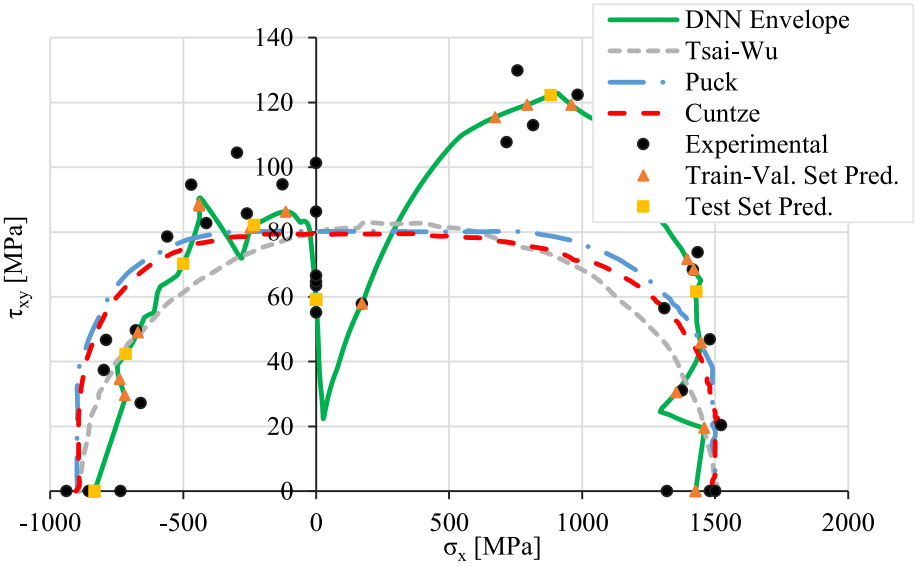

Fig. A.2. Neural network experimental data and failure envelope predictions compared to conventional failure criteria for WWFE-I test case 2.

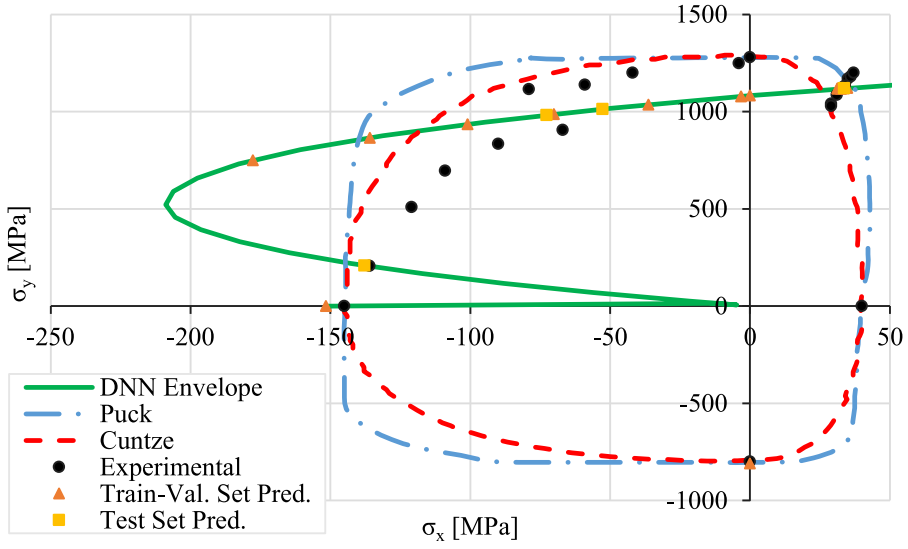

Fig. A.3. Neural network experimental data and failure envelope predictions compared to conventional failure criteria for WWFE-I test case 3.

Data availability

Data for this research are taken from Soden et al. (2004b), Lee et al. (1999), and Hinton and Kaddour (2013).

Acknowledgment

This work was supported by the Natural Sciences and Engineering Research Council of Canada (NSERC).

Appendix A

See Figs. A.1–A.13.

Appendix B

See Table B.1.

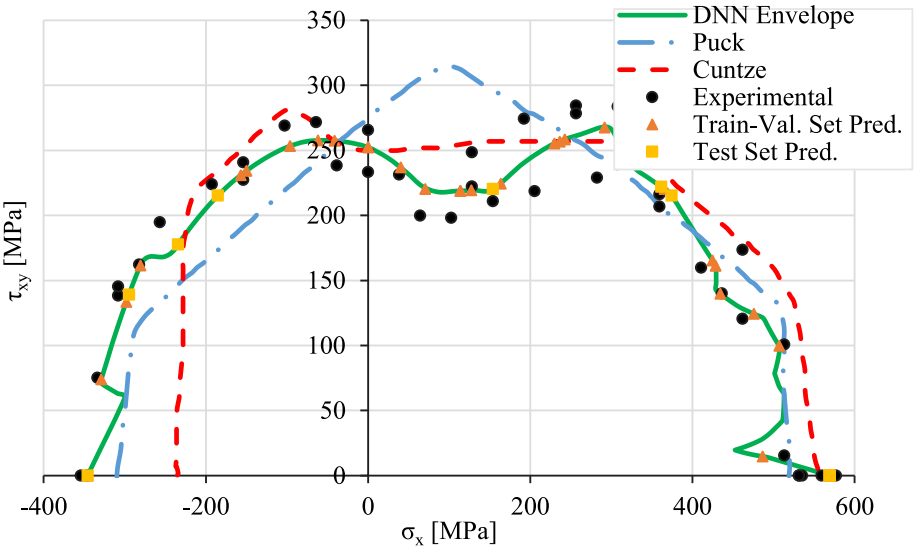

Fig. A.4. Neural network experimental data and failure envelope predictions compared to conventional failure criteria for WWFE-I test case 5.

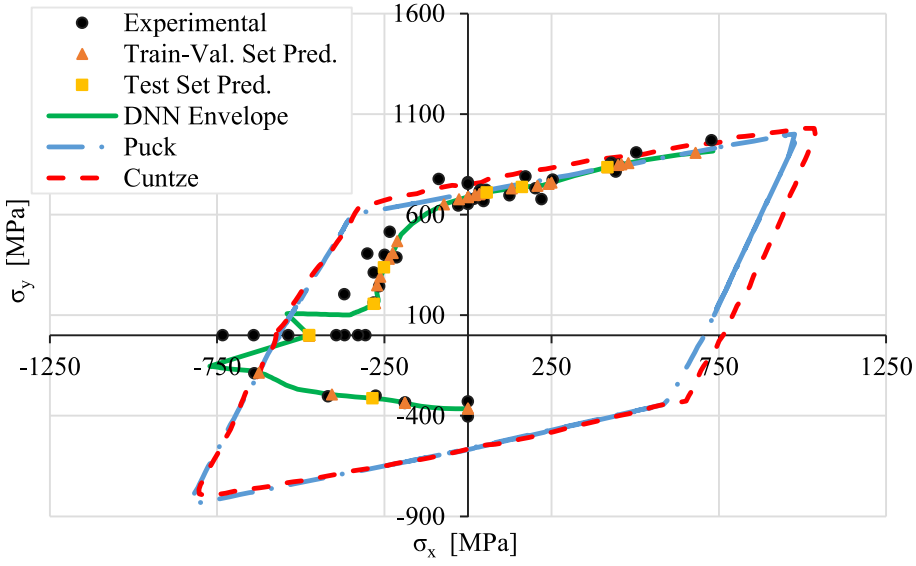

Fig. A.5. Neural network experimental data and failure envelope predictions compared to conventional failure criteria for WWFE-I test case 6.

Table B.1
Data matrix example.

Pt. #	σ_{1T}	σ_{1C}	σ_{2T}	σ_{2C}	σ_{3T}	σ_{3C}	τ_{12}	τ_{13}	τ_{23}	S. Y/N	σ_x	σ_y	σ_z	τ_{xy}	τ_{xz}	τ_{yz}	Ply 1	Ply2	Ply 3	Ply 4
1	1950	1480	48	200	48	200	79	79	79	1	0.75	1	0	0	0	0	0	+45	−45	90
2	1140	570	35	114	35	114	72	72	72	1	1.74	0	0	1	0	0	90	+30	−30	90
3	2560	1590	73	185	63	185	90	90	57	1	0	0	−0.52	0	0	1	90	+45	−45	0

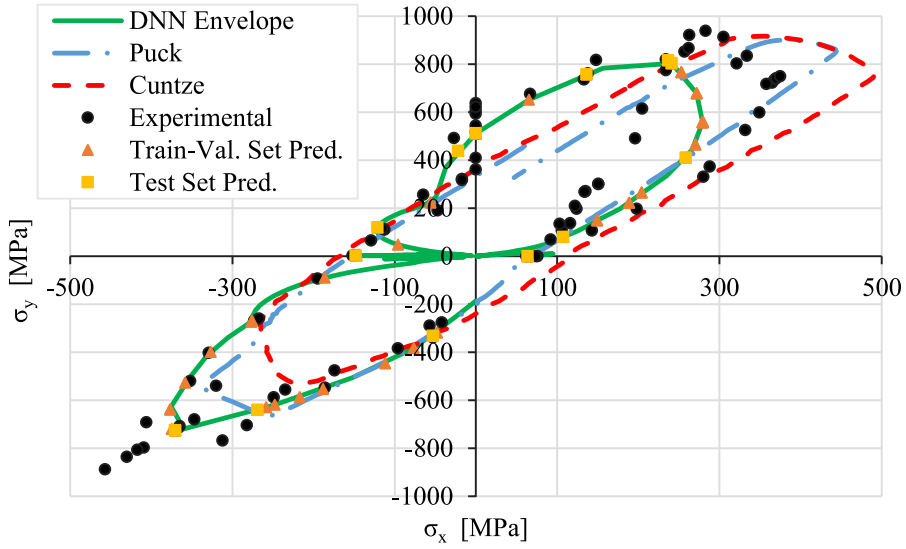

Fig. A.6. Neural network experimental data and failure envelope predictions compared to conventional failure criteria for WWFE-I test case 7.

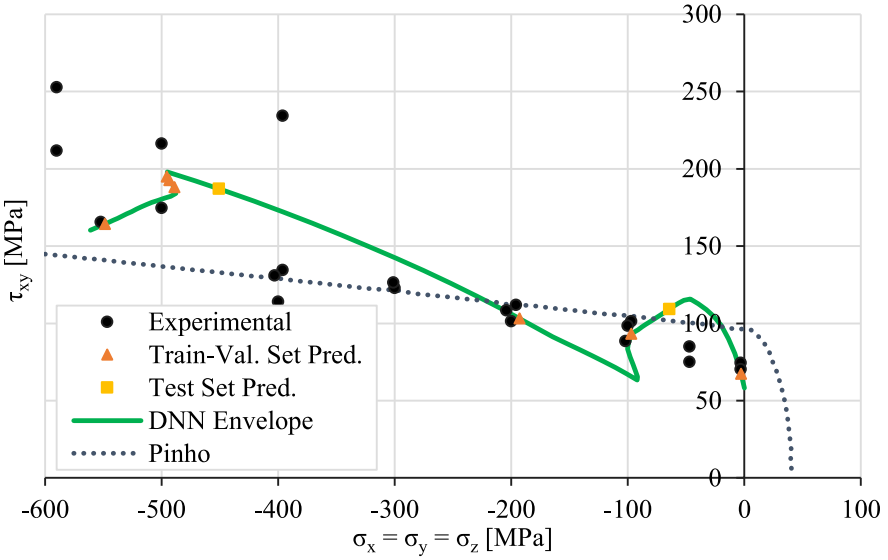

Fig. A.7. Neural network experimental data and failure envelope predictions compared to conventional failure criteria for WWFE-II test case 9.

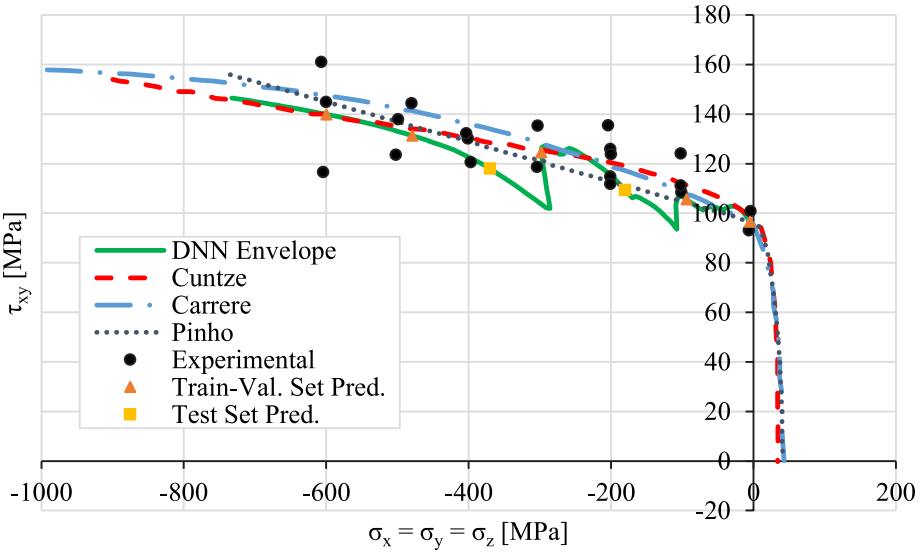

Fig. A.8. Neural network experimental data and failure envelope predictions compared to conventional failure criteria for WWFE-II test case 10.

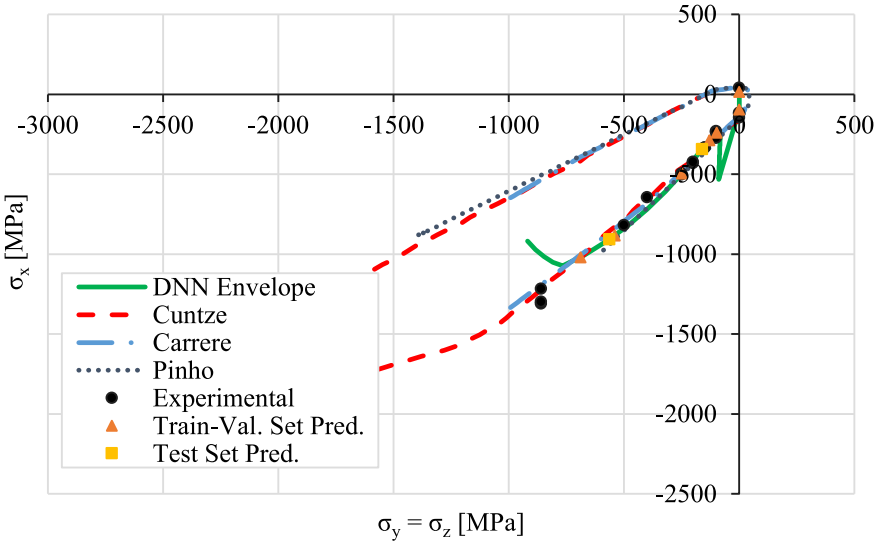

Fig. A.9. Neural network experimental data and failure envelope predictions compared to conventional failure criteria for WWFE-II test case 11.

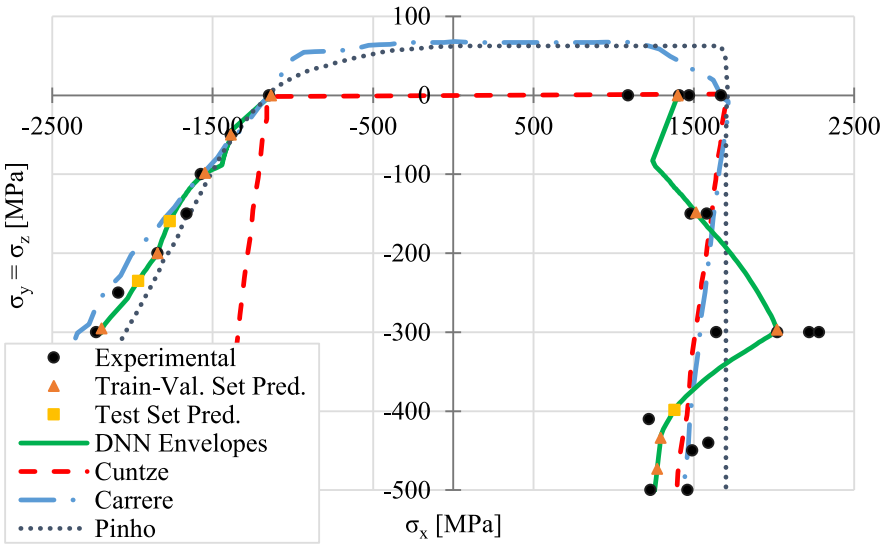

Fig. A.10. Neural network experimental data and failure envelope predictions compared to conventional failure criteria for WWFE-II test case 12.

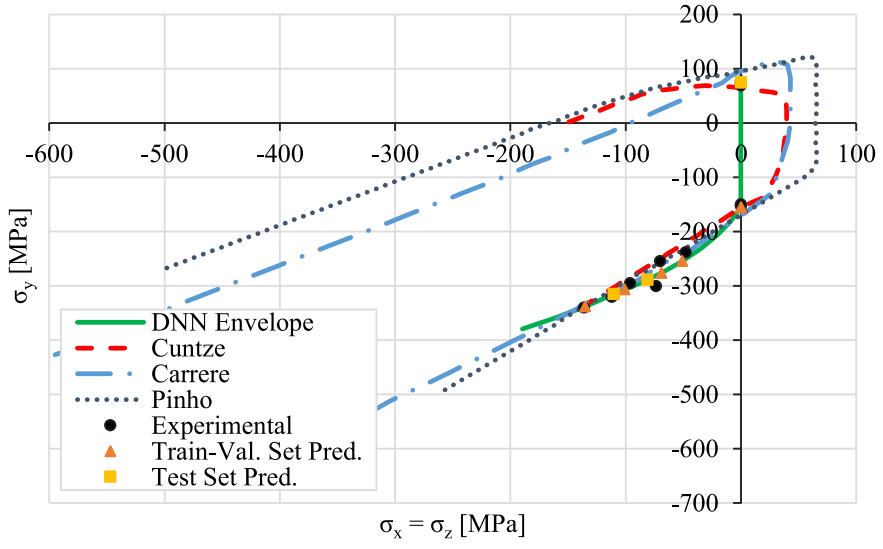

Fig. A.11. Neural network experimental data and failure envelope predictions compared to conventional failure criteria for WWFE-II test case 14.

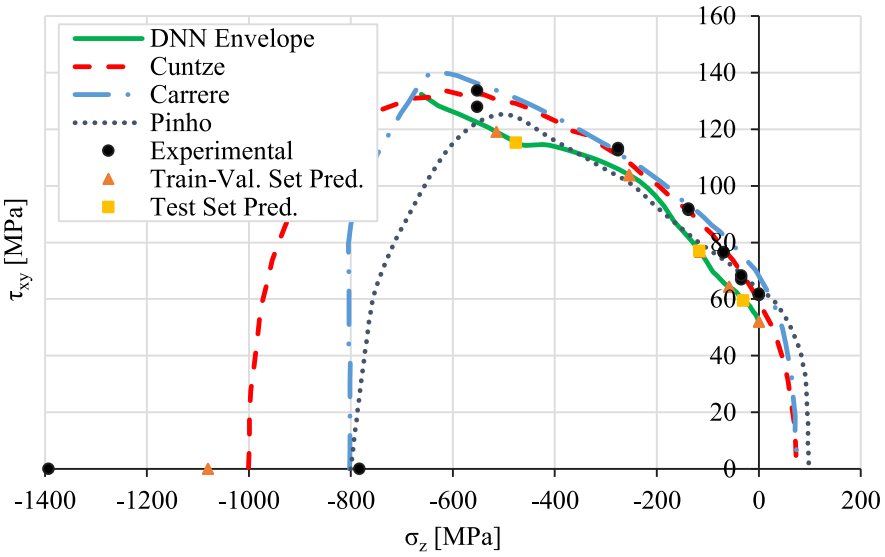

Fig. A.12. Neural network experimental data and failure envelope predictions compared to conventional failure criteria for WWFE-II test case 15.

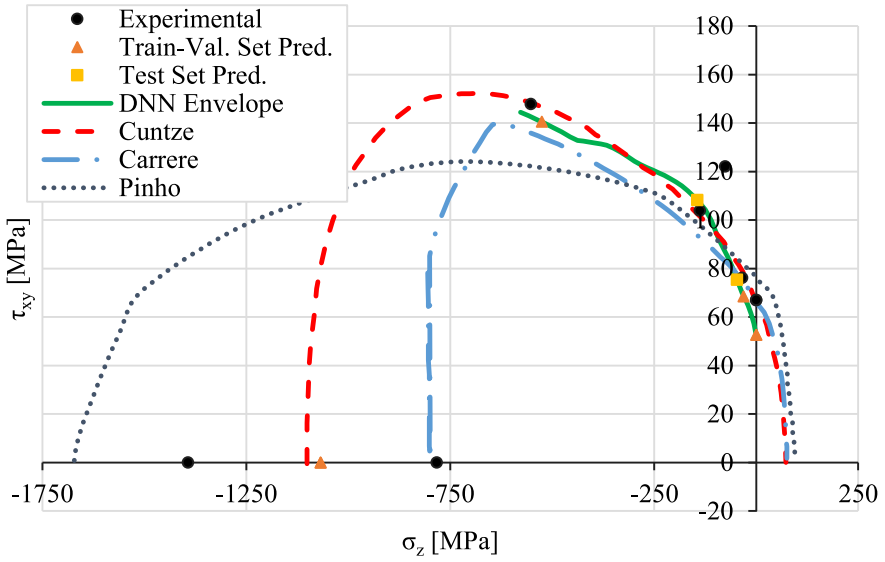

Fig. A.13. Neural network experimental data and failure envelope predictions compared to conventional failure criteria for WWFE-II test case 16.

References

Al-Assadi, M., El Kadi, H.A., Deiab, I.M., 2010. Using artificial neural networks to predict the fatigue life of different composite materials including the stress ratio effect. Appl. Compos. Mater. 18, 297–309.

Aleksendrić, D., Carlone, P., Ćirović, V., 2016. Optimization of the temperature-time curve for the curing process of thermoset matrix composites. Appl. Compos. Mater. 23, 1047–1063. http://dx.doi.org/10.1007/s10443-016-9499-y.

Carrere, N., Laurin, F., Maire, J.-F., 2012. Micromechanical-based hybrid mesoscopic 3D approach for non-linear progressive failure analysis of composite structures. J. Compos. Mater. 46, 2389–2415. http://dx.doi.org/10.1177/0021998312450179.

Carrere, N., Laurin, F., Maire, J.-F., 2013. Micromechanical-based hybrid mesoscopic three-dimensional approach for non-linear progressive failure analysis of composite structures—Part B: Comparison with experimental data. J. Compos. Mater. 47, 743–762. http://dx.doi.org/10.1177/0021998312460558.

Chen, J., Wan, L., Ismail, Y., Ye, J., Yang, D., 2021. A micromechanics and machine learning coupled approach for failure prediction of unidirectional CFRP composites under triaxial loading: A preliminary study. Compos. Struct. 267, 113876. http://dx.doi.org/10.1016/j.compstruct.2021.113876.

Cuntze, R.G., 2004. Chapter 5.13 - The predictive capability of failure mode concept-based strength criteria for multi-directional laminates—Part B. In: Hinton, M.J., Kaddour, A.S., Soden, P.D. (Eds.), Failure Criteria in Fibre-Reinforced-Polymer Composites. Elsevier, Oxford, pp. 976–1025. http://dx.doi.org/10.1016/B978-008044475-8/50035-4.

Cuntze, R., 2012. The predictive capability of failure mode concept-based strength conditions for laminates composed of unidirectional laminae under static triaxial stress states. J. Compos. Mater. 46, 2563–2594. http://dx.doi.org/10.1177/0021998312449894.

Cuntze, R., 2013. Comparison between experimental and theoretical results using Cuntze's failure mode concept model for composites under triaxial loadings—Part B of the second world-wide failure exercise. J. Compos. Mater. 47, 893–924. http://dx.doi.org/10.1177/0021998312456409.

Fan, H.-T., Wang, H., 2014. Predicting the open-hole tensile strength of composite plates based on probabilistic neural network. Appl. Compos. Mater. Int. J. Sci. Appl. Compos. Mater. 21, 827–840. http://dx.doi.org/10.1007/s10443-014-9387-2.

Fernández, J., Chiachío, M., Chiachío, J., Muñoz, R., Herrera, F., 2022. Uncertainty quantification in neural networks by approximate Bayesian computation: Application to fatigue in composite materials. Eng. Appl. Artif. Intell. 107, 104511. http://dx.doi.org/10.1016/j.engappai.2021.104511.

Fontes, A., Shadmehri, F., 2021. Failure prediction of composite materials using deep neural networks. In: 36th Annual Technical Conference of the American Society for Composites. Presented at the 36th Annual Technical Conference of the American Society for Composites. DEStech Publications, Inc., College Station, Texas, USA, pp. 1068–1079.

Goodfellow, I., Bengio, Y., Courville, A., 2016. Deep learning. In: Adaptive Computation and Machine Learning. The MIT Press, Cambridge, Massachusetts.

2019. Google colaboratoy.

Gurney, K., 1997. An Introduction to Neural Networks. UCL Press, London.

Hinton, M., Kaddour, A., 2012. The background to the second world-wide failure exercise. J. Compos. Mater. 46, 2283–2294. http://dx.doi.org/10.1177/0021998312449885.

Hinton, M., Kaddour, A., 2013. Triaxial test results for fibre-reinforced composites: The second world-wide failure exercise benchmark data. J. Compos. Mater. 47, 653–678. http://dx.doi.org/10.1177/0021998312459782.

Hinton, M.J., Kaddour, A.S., Soden, P.D., 2004. Chapter 1.1 - The world-wide failure exercise: Its origin, concept and content. In: Hinton, M.J., Kaddour, A.S., Soden, P.D. (Eds.), Failure Criteria in Fibre-Reinforced-Polymer Composites. Elsevier, Oxford, pp. 2–28. http://dx.doi.org/10.1016/B978-008044475-8/50002-0.

Humfeld, K.D., Gu, D., Butler, G.A., Nelson, K., Zobeiry, N., 2021. A machine learning framework for real-time inverse modeling and multi-objective process optimization of composites for active manufacturing control. Composites B 223, 109150. http://dx.doi.org/10.1016/j.compositesb.2021.109150.

Islam, F., Wanigasekara, C., Rajan, G., Swain, A., Prusty, B.G., 2022. An approach for process optimisation of the Automated Fibre Placement (AFP) based thermoplastic composites manufacturing using machine learning, photonic sensing and thermo-mechanics modelling. Manuf. Lett. 32, 10–14. http://dx.doi.org/10.1016/j.mfglet.2022.01.002.

Kaddour, A., Hinton, M., 2012. Input data for test cases used in benchmarking triaxial failure theories of composites. J. Compos. Mater. 46, 2295–2312. http://dx.doi.org/10.1177/0021998312449886.

Kaddour, A., Hinton, M., 2013. Maturity of 3D failure criteria for fibre-reinforced composites: Comparison between theories and experiments: Part B of WWFE-II. J. Compos. Mater. 47, 925–966. http://dx.doi.org/10.1177/0021998313478710.

Ketkar, N., 2017. Deep Learning with Python : A Hands-on Introduction. A Press, United States, http://dx.doi.org/10.1007/978-1-4842-2766-4.

Kuraishi, A., Tsai, S.W., Liu, K.K.S., 2004. Chapter 5.9 - A progressive quadratic failure criterion, part B. In: Hinton, M.J., Kaddour, A.S., Soden, P.D. (Eds.), Failure Criteria in Fibre-Reinforced-Polymer Composites. Elsevier, Oxford, pp. 903–921. http://dx.doi.org/10.1016/B978-008044475-8/50031-7.

Labossière, P., Turkkan, N., 1993. Failure prediction of fibre-reinforced materials with neural networks. J. Reinf. Plast. Compos. 12, 1270–1280. http://dx.doi.org/10.1177/073168449301201202.

Lee, C.S., Hwang, W., Park, H.C., Han, K.S., 1999. Failure of carbon/epoxy composite tubes under combined axial and torsional loading 1. Experimental results and prediction of biaxial strength by the use of neural networks. Compos. Sci. Technol. 59, 1779–1788. http://dx.doi.org/10.1016/S0266-3538(99)00038-X.

Niaki, S.A., Haghighat, E., Campbell, T., Poursartip, A., Vaziri, R., 2021. Physics-informed neural network for modelling the thermochemical curing process of composite-tool systems during manufacture. Comput. Methods Appl. Mech. Engrg. 384, 113959. http://dx.doi.org/10.1016/j.cma.2021.113959.

Paszke, A., Gross, S., Massa, F., Lerer, A., Bradbury, J., Chanan, G., Killeen, T., Lin, Z., Gimelshein, N., Antiga, L., Desmaison, A., Kopf, A., Yang, E., DeVito, Z., Raison, M., Tejani, A., Chilamkurthy, S., Steiner, B., Fang, L., Bai, J., Chintala, S., 2019. Pytorch: An imperative style, high-performance deep learning library. In: Wallach, H., Larochelle, H., Beygelzimer, A., Alché-Buc, F., d' Fox, E., Garnett, R. (Eds.), Advances in Neural Information Processing Systems 32. Curran Associates, Inc., pp. 8024–8035.

Pinho, S., Darvizeh, R., Robinson, P., Schuecker, C., Camanho, P., 2012. Material and structural response of polymer–matrix fibre-reinforced composites. J. Compos. Mater. 46, 2313–2341. http://dx.doi.org/10.1177/0021998312454478.

Pinho, S., Vyas, G., Robinson, P., 2013. Material and structural response of polymer–matrix fibre-reinforced composites: Part B. J. Compos. Mater. 47, 679–696. http://dx.doi.org/10.1177/0021998313476523.

Puck, A., Schürmann, H., 2004. Chapter 5.6 - Failure analysis of FRP laminates by means of physically based phenomenological models. In: Hinton, M.J., Kaddour, A.S., Soden, P.D. (Eds.), Failure Criteria in Fibre-Reinforced-Polymer Composites. Elsevier, Oxford, pp. 832–876. http://dx.doi.org/10.1016/B978-008044475-8/50028-7.

2018. Python.

Raschka, Sebastian, Liu, Yuxi (Hayden), Mirjalili, V., 2022. Machine Learning with PyTorch and Scikit-Learn. Packt Publishing, Birmingham, UK.

Sapuan, S.M., Mujtaba, I.M., 2009. Composite Materials Technology : Neural Network Applications. Taylor & Francis Group, Baton Rouge, United States.

Seyhan, A.T., Tayfur, G., Karakurt, M., Tanoglu, M., 2005. Artificial neural network (ANN) prediction of compressive strength of VARTM processed polymer composites. Comput. Mater. Sci. 34, 99–105. http://dx.doi.org/10.1016/j.commatsci.2004.11.001.

Soden, P.D., Hinton, M.J., Kaddour, A.S., 2004a. Chapter 2.1 - Lamina properties, lay-up configurations and loading conditions for a range of fibre reinforced composite laminates. In: Failure Criteria in Fibre-Reinforced-Polymer Composites. Elsevier, Oxford, pp. 30–51. http://dx.doi.org/10.1016/B978-008044475-8/50003-2.

Soden, P.D., Hinton, M.J., Kaddour, A.S., 2004b. Chapter 2.2 - Biaxial test results for strength and deformation of a range of E-glass and carbon fibre reinforced composite laminates. In: Failure Exercise Benchmark Data, Failure Criteria in Fibre-Reinforced-Polymer Composites. Elsevier, Oxford, pp. 52–96. http://dx.doi.org/10.1016/B978-008044475-8/50004-4.

Soden, P., Kaddour, A.S., Hinton, M., 2004. Chapter 7.1 - Recommendations for designers and researchers resulting from the world-wide failure exercise. In: Failure Criteria in Fibre-Reinforced-Polymer Composites. pp. 1223–1251. http://dx.doi.org/10.1016/B978-008044475-8/50039-1.

Stamopoulos, A.G., Tserpes, K.I., Dentsoras, A.J., 2018. Quality assessment of porous CFRP specimens using X-ray computed tomography data and artificial neural networks. Compos. Struct. 192, 327–335. http://dx.doi.org/10.1016/j.compstruct.2018.02.096.

Tang, Y., Wang, Q., Cheng, L., Li, J., Ke, Y., 2022. An in-process inspection method integrating deep learning and classical algorithm for automated fiber placement. Compos. Struct. 300, 116051. http://dx.doi.org/10.1016/j.compstruct.2022.116051.

Tsai, S.W., Wu, E.M., 1971. A general theory of strength for anisotropic materials. J. Compos. Mater. 5, 58–80. http://dx.doi.org/10.1177/002199837100500106.

Wanigasekara, C., Oromiehie, E., Swain, A., Prusty, B.G., Nguang, S.K., 2020. Machine learning based predictive model for AFP-based unidirectional composite laminates. IEEE Trans. Ind. Inform. 16, 2315–2324. http://dx.doi.org/10.1109/TII.2019.2932398.

Wanigasekara, C., Oromiehie, E., Swain, A., Prusty, B.G., Nguang, S.K., 2021. Machine learning-based inverse predictive model for AFP based thermoplastic composites. J. Ind. Inf. Integr. 22, 100197. http://dx.doi.org/10.1016/j.jii.2020.100197.